Human Reproduction, Vol.26, No.6 pp. 1408–1421, 2011
Advanced Access publication on March 18, 2011 doi:10.1093/humrep/der057

human reproduction

ORIGINAL ARTICLE *Reproductive biology*

Dynamics of the primate ovarian surface epithelium during the ovulatory menstrual cycle

Jay W. Wright [1,2,*], Leigh Jurevic [1], and Richard L. Stouffer [1,2]

[1]Division of Reproductive Sciences, Oregon National Primate Research Center, Beaverton, OR 97006, USA [2]Department of Obstetrics and Gynecology, Oregon Health & Science University, Portland, OR 97201, USA

*Correspondence address. Tel: +1-503-690-5316; Fax: +1-503-690-5563; Email: wrightj@ohsu.edu

Submitted on December 8, 2010; resubmitted on January 29, 2011; accepted on February 9, 2011

BACKGROUND: Epithelial ovarian cancer (EOC) risk correlates strongly with the number of ovulations that a woman experiences. The primary source of EOC in women is the ovarian surface epithelium (OSE). Mechanistic studies on the etiology of OSE transformation to EOC cannot be realistically performed in women. Selecting a suitable animal model to investigate the normal OSE in the context of ovulation should be guided by the model's reproductive similarities to women in natural features that are thought to contribute to EOC risk.

METHODS: We selected the non-human primate, rhesus macaque, as a surrogate to study the normal OSE during the natural menstrual cycle. We investigated OSE morphology and marker expression, plus cell proliferation and death in relation to menstrual cycle stage and ovulation.

RESULTS: OSE cells displayed a morphological range from squamous to columnar. Cycle-independent parameters and cycle-dependent changes were observed for OSE histology, steroid receptor expression, cell death, DNA repair and cell adhesion. Contrary to findings in non-primates, primate OSE cells were not manifestly cleared from the site of ovulation, nor were proliferation rates affected by ovulation or stage of the menstrual cycle. DNA repair proteins were more highly expressed in OSE than in other ovarian cells.

CONCLUSIONS: This study identifies significant differences between primate and non-primate OSE. In contrast to established views, ovulation-induced death and proliferation are not indicated as prominent contributors to EOC risk, but disruption of OSE cadherin-mediated adhesion may be, as could the loss of ovary-mediated chronic suppression of proliferation and elevation of DNA repair potential.

Key words: epithelial ovarian cancer / ovarian surface epithelium / non-human primate / menstrual cycle / cadherin

Introduction

The ovarian surface epithelium (OSE) is a discreet layer of cells surrounding the ovary and is the primary source of ovarian cancer in women (Wong and Auersperg, 2003; Auersperg *et al.*, 2008). The lifetime risk for epithelial ovarian cancer (EOC) is 1–2%, despite the fact that the entire population of OSE cells is only about 10^7 cells per ovary. The molecular basis for why the OSE is so highly prone to transformation is not understood, but because the major risk factors for the disease are age, menopause, ovarian function and genetics (Sueblinvong and Carney, 2009), it would appear that a woman's natural biology places these cells at risk. A considerable body of data from human tissues, cell culture experiments and animal studies provides rationale for how these factors may promote EOC: (i) the frequency of premalignant inclusion cysts correlates positively with age and the total number of ovulations a woman experiences (Westhoff *et al.*, 1993; Heller *et al.*, 2005; Tan *et al.*, 2005); (ii) progestins can induce OSE apoptosis *in vivo* (Rodriguez *et al.*, 2002); (iii) cultured OSE and ovarian cancer cells respond to high concentrations of estradiol and progesterone (E and P) by growth arrest and up-regulation of apoptotic indicators (Keith Bechtel and Bonavida, 2001; Wright et al., 2005), or by increased proliferation *in vivo* (Bai *et al.*, 2000); (iv) gonadotrophins that regulate ovarian function can promote proliferation in cultured OSE cells and *in vivo* (Davies *et al.*, 1999; Ivarsson *et al.*, 2001; Parrott *et al.*, 2001); (v) ovulation is accompanied by wound/inflammatory processes that are genotoxic (Gubbay *et al.*, 2005; Rae and Hillier, 2005; Fegan *et al.*, 2008); (vi) prior to ovulation, ovarian factors inflict genetic damage and death on the OSE (Colgin and Murdoch, 1997; Murdoch *et al.*, 2001; Murdoch and Martinchick, 2004), whereas after ovulation, increased proliferation in the OSE has been detected (Osterholzer *et al.*, 1985; Bai *et al.*, 2000); and (vii) models of superovulation show increased OSE proliferation and inclusion cyst formation (Burdette *et al.*, 2006, 2007).

Determining how and to what extent ovarian function affects EOC risk and drives OSE transformation in women is important for understanding disease origins and progression, and to assess risk of clinical treatments, particularly fertility and hormone therapies. It is not feasible to study the OSE of women during the natural menstrual cycle or under controlled experimental conditions. Most species, including mice, sheep and rabbits in studies cited above, do not develop EOC spontaneously, possibly owing to basic reproductive differences that affect the OSE, and thus may not be well-suited to study how natural risk factors contribute to its transformation. The rhesus macaque, a non-human primate, may offer a suitable alternative model. Rhesus monkey females have genetic and physiological characteristics similar to women, including a 28-day menstrual cycle, comparable sex steroid and gonadotrophin regulation of the ovary, a reproductive life spanning decades and menopause; in addition, spontaneous EOC has been detected in the non-human primate, including the rhesus monkey [reported in (Moore *et al*., 2003)].

On the basis of available data, it may be hypothesized that the human OSE undergoes dynamic regulation during the natural menstrual cycle, as seen in non-primates. This could include up- and down-regulation of E and P receptors in response to cyclic patterns of E and P production (Chaffin *et al*., 1999; Mukherjee *et al*., 2005; Giles *et al*., 2006); low basal levels of proliferation (Werness *et al*., 1999; Heller *et al*., 2003; Piek *et al*., 2003; Slot *et al*., 2006; Pothuri *et al*., 2010), punctuated by higher levels following ovulation (Osterholzer *et al*., 1985; Bai *et al*., 2000; Doyle and Donadeu, 2009), and; increased cell death prior to ovulation and in the presence of high levels of P produced by the corpus luteum (CL) (Murdoch *et al*., 2001; Rodriguez *et al*., 2002). Changes in cellular morphology may also occur as the ovarian surface expands and contracts in response to follicle growth, ovulation and luteal regression. Studying the rhesus macaque OSE may, or may not, confirm findings from other species and help define how the menstrual cycle contributes to EOC in women.

Therefore, experiments were designed to investigate the rhesus macaque OSE during the menstrual cycle, and in relation to the dominant follicle selected to ovulate and the CL. We observed cyclic changes in cell morphology and adhesion, E and P receptor expression, cell cycle arrest and death and DNA repair protein expression. In contrast to reports detailing the non-primate OSE, we did not observe cell death or proliferation localized to the follicle rupture site. Expression levels of two DNA repair proteins, FANCD2 and Ogg1, were chronically higher in OSE than other ovarian cell types.

It should be noted that an accumulation of convincing data indicate an alternative source of high grade pelvic tumors diagnosed as EOC, in the fimbrial epithelium (FE). Genetic similarity between OSE, FE and these tumors has been reported (Marquez *et al*., 2005), and putative early lesions have been identified in the distal fallopian tube and fimbria of women, primarily those with BRCA1 mutations, after undergoing prophylactic salpingo-oophorectomy (Medeiros *et al*., 2006; Folkins *et al*., 2009). Challenges that exist for studying the OSE of women also apply to investigations of the FE, and the non-human primate may be well-suited for such investigations; however, the current study is focused on the primate OSE.

Our findings indicate that some hypotheses on the early etiology of EOC are not well supported and that the primate OSE may be unique in some regards, most notably by a lack of destruction and proliferation within the OSE in response to ovulation. As a consequence, despite the power of some animal model systems that spontaneously develop EOC [the hen; (Fredrickson, 1987; Johnson, 2009)] or else are accessible to genetic manipulation to simulate OSE malignancy [the mouse; (Fong and Kakar, 2009)], the non-human primate may be best suited as a surrogate for women to investigate precancerous OSE and early EOC etiology, and for the development of novel strategies for prevention and early detection.

Materials and Methods

Animal care and menstrual cycle staging

Rhesus monkeys (*Macaca mulatta*) were housed and cared for at the Oregon National Primate Research Center (ONPRC) on the West Campus of the Oregon Health & Science University (OHSU), as described previously (Wolf *et al*., 1990). Protocols were approved by the ONPRC/OHSU Animal Care and Use Committee, in accordance with the National Institute of Health guidelines ((NRC), 1996). Adult female monkeys ($n = 17$) 6–16 years of age were selected for the current study. The reproductive age for rhesus monkey females begins at ~3 years of age (menarche) and lasts until menopause, in the early-to-mid 20s (Bellino and Wise, 2003; Nichols *et al*., 2005; Walker and Herndon, 2008). The median age at which ovarian carcinomas occur in rhesus monkeys has not been accurately recorded, but is generally in 'adult', 'mature' and 'old' females, though has been reported as early as 2 years of age [reported in (Moore *et al*., 2003)]. Menstrual cycles were staged using at least two of the following three methods: visual evidence of menses, serum assays of E (17-ß-estradiol) and P, and ovarian histology. Serum levels of E and P were determined by fluorescent assay using an IMMULITE 2000 (Seimens Medical Solutions, Malvern, PA, USA) in the ONPRC Endocrine Technology and Support Core (Young *et al*., 2002).

Tissue collection

Cycling rhesus macaques have a 24–31-day (mean 28) menstrual cycle (Resko *et al*., 1982; Lane *et al*., 2001). Day 1 was defined as the first day of menses. Ovaries were collected during the perimenstrual (PM) stage between Day 25 and Day 3 ($n = 4$ ovaries), the time of dominant follicle development (DF) from Day 4 to 10 ($n = 5$), during the periovulatory stage (PO) from Day 11 to 17 ($n = 6$), or during the subsequent interval of CL steroidogenesis, between Days 18 and 24 ($n = 4$). Contralateral ovaries with no dominant follicle or CL (ND; $n = 8$) were also collected. Additional ovaries were collected from three monkeys that were not cycling, due to season, to obtain OSE RNA representing a baseline of *in vivo* gene expression. These were selected as controls rather than prepubescent or post-menopausal females, which would have either never experienced hormonal cycles or experienced depletion of E and P and sustained elevation of FSH and LH. The hormonal milieu of non-cycling adults is considered the most appropriate baseline control. Ovaries were collected laparoscopically by veterinary staff in the ONPRC Division of Animal Resources from anesthetized animals and placed in sterile saline or saline with 18% formaldehyde and 0.1% Triton.

OSE histology, immunohistochemical labeling and analysis

Fixed ovaries were paraffin embedded and cut into 5 μm sections as described previously (Wright *et al*., 2010) for hematoxylin and eosin (H&E) or immunohistochemical (IHC) staining. H&E labeled sections were used to examine OSE morphological characteristics: height, lateral density and presence or absence of an apical projection. Cells were

defined as Type 1, 2 or 3, on the basis of height, with Type 1 <2.5 μm, Type 2 between 2.5 and 7.5 μm and Type 3 >7.5 μm. Apical projections were excluded from height measurements. Fields of view (FOV) of 500 μm in OSE length were scored for predominant morphological type, and percentage of cells bearing an apical projection. Cell density was quantified as the number of OSE cells per 250 μm of ovarian surface length, from 30 FOV selected randomly among all ovaries at all stages, or from 5 FOV that represented each individual morphological Type.

IHC was conducted as described (Wright *et al.*, 2008, 2010), with modified antigen retrieval by pressure cooking for 30 min in Citra Solution (BioGenex; San Ramon, CA, USA). A minimum of three sections from each ovary for each antibody was examined. Primary antibodies against the following antigens were used: keratin, estrogen receptor-alpha (ER-α) and progesterone receptor (PR; DAKO Corp.; Carpinteria, CA, USA), ER-β (Affinity Bioreagents; Golden, CO, USA), progesterone receptor membrane component-1 (PGRMC1; Abcam; Cambridge, MA, USA), E- and N-Cadherin (BD Transduction Laboratories; San Jose, CA, USA), P-Cadherin (Sigma-Aldrich; St Louis, MO, USA), OB-Cadherin (Invitrogen; Carlsbad, CA, USA), PCNA and phospho-histone 3 (pH3; Chemicon International; Temecula, CA, USA), phospho-Retinoblastoma (pRb), p21 and cleaved caspase-3 (Cell Signaling Technology, Inc.; Danvars, MA, USA), p53 (Calbiochem; Gibbstown, NJ, USA), and Fanconi anemia D2 (FANCD2) and oxoguanine glycosylase (Ogg1; Novus Biologicals; Littleton, CO, USA). Phosphatase-conjugated secondary antibodies and colorimetric reagents were from Kirkegaard & Perry Laboratories (Gaithersburg, MD, USA).

Visual examination of each section at 100–960× magnification was conducted using an Olympus IX71 inverted microscope (Olympus; Center Valley, PA, USA), and photo imaging was performed using an Olympus Microfire camera connected to an Apple iMac G5 (Apple; Cupertino, CA, USA) operating PictureFrame 2.0 (Optronics; Goleta, CA, USA). Antigen expression was quantified as the percentage of OSE cells expressing signal, as indicated by colorimetric precipitate greater than in negative controls; i.e. sections exposed to secondary antibody alone. Quantification of staining intensity was not performed.

RNA purification and analysis

The ovarian surfaces of six ovaries from three females were brushed to collect OSE cells, as described (Wright *et al.*, 2008), except that the ovaries were removed from the females and the entire epithelium was collected. Total RNA was purified using an RNeasy kit (Qiagen; Valencia, CA, USA) per manufacturer's instructions. OSE RNA from both ovaries from each female was pooled, so three separate OSE RNA samples were sent to the OHSU Gene Microarray Shared Resource Affymetrix Microarray Core for quality control, labeling, hybridization to GeneChip Rhesus Macaque Genome Arrays (Affymetric, Inc.; Santa Clara, CA, USA) and data management (Bogan *et al.*, 2008). For the current study, only properly annotated probe sets (National Center for Biotechnology Information and University of Nebraska Non-Human Primate Genomics Center) corresponding to cadherin isoforms were included.

Statistical analysis

Differences in OSE histology and antigen expression between stages in the natural menstrual cycle and in relation to the dominant follicle or corpus lutem were analyzed by analysis of variance, followed by Student's *t*-test where appropriate. Statistical software used was SigmaStat 2.0 (Systat Software; San Jose, CA, USA), Microsoft Excel 2008 (Microsoft; Redmond, WA, USA) and iWork Numbers '09 (Apple; Cupertino, CA, USA).

Results

OSE histology

Primate OSE cells exhibited a range of sizes (Fig. 1A), distinguishable on the basis of height (Fig. 1B), lateral density (Fig. 1C) and the presence of an apical projection (Fig. 1D). The frequency of Types varied during the menstrual cycle (Fig. 1B), with Type 1 cells showing a trend ($P = 0.1$) to rise between the DF and CL stages, Type 2 cells significantly ($P < 0.05$) increasing from PM to DF and tending ($P = 0.1$) to decline between DF and CL and a trend ($P = 0.09$) for in Type 3 cells to decline from PM to DF. Generally, 13.5 ± 14.2% of cells were Type 1, 79.4 ± 20.1% were Type 2 and 6.8 ± 12% were Type 3. The lateral density of these Types differed from each other (Fig. 1C), with Type 1 cells being significantly ($P < 0.01$) less dense and Type 3 ($P < 0.05$) being more dense than Type 2 cells. Apical projections were observed in 45 ± 12% of Type 2 cells and 65 ± 21% of Type 3 cells, but not in Type 1 cells. No significant relationship was seen between cell type and proximity to the dominant follicle or CL, except that Type 3 cells were not seen over the pre-ovulatory follicle.

Cadherin isoform expression in the primate OSE

Microarray data provided a cadherin gene expression profile (Fig. 2) more detailed than previously reported for non-human primates (Wright *et al.*, 2008), and in agreement with recently available human OSE gene expression data [http://www.ncbi.nlm.nih.gov/gds; reference series GSE14407 (Bowen *et al.*, 2009)]. In non-cycling females ($n = 3$), robust levels of CDH1, 2, 3 and 11 (E-, N-, P- and OB-cadherin, respectively) mRNAs were observed in the OSE. These were selected for further study using IHC. Nine other isoforms were reported as present, whereas 10 isoforms were absent. Note that the gene symbol numbering omits CDH14, 21 and 25.

E-cadherin in a Day 8 OSE: an illustration of intraovarian variation

Analysis of individual FOV ~2 mm in length in 14 tissue sections, collected at 150 μm intervals from a Day 8 ovary (Fig. 3A and B), revealed intraovarian variation in the percentage of OSE cells staining positive for E-cadherin. Values ranged from 0 to 100% of cells within FOVs in the two panels shown (Fig. 3B). Segregating FOV on the basis of proximity to the dominant follicle did not reveal consistent significant differences in expression levels on the basis of this proximity. Note that the sections shown (Fig. 3B; #9 and 12, corresponding to sections 373 and 463) were spaced ~0.45 mm apart and the dominant follicle was of similar size (5.6 and 5.1 mm in diameter, respectively) and proximity to the surface (0.35 and 0.46 mm, respectively) in both sections, yet the percentage of E-cadherin-positive cells in the vicinity of the dominant follicle varied widely between these two sections.

When data from all 14 sections spanning this ovary were compiled, a more comprehensive profile of expression was generated (Fig. 3C), revealing an overall expression of E-cadherin by 21.6 ± 12.3% of all OSE cells associated with this ovary. The percentage of OSE cells close to the dominant follicle that were positive for E-cadherin was

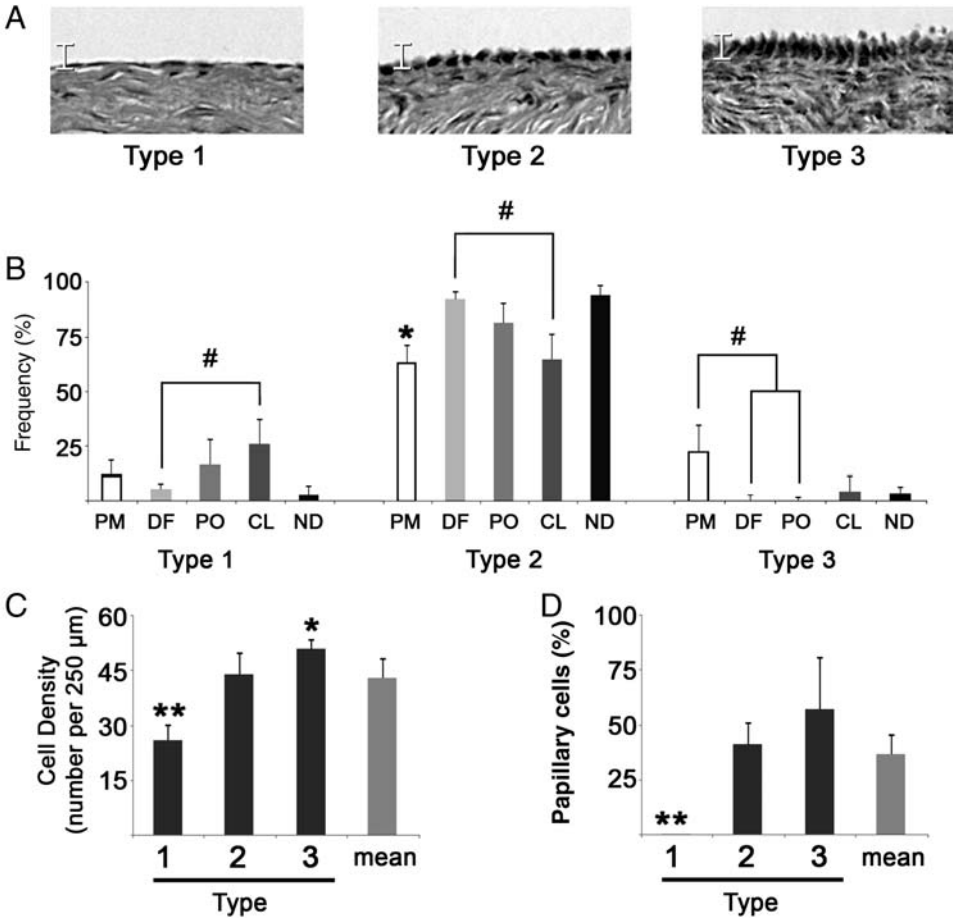

Figure 1 Frequency and density of OSE morphological types and cells with apical projections. (**A**) Images display representative examples of Type 1, 2 or 3 OSE cells. Scale bracket is 10 μm. (**B**) Histograms summarize the frequency of each type in relation to the stage of the natural menstrual cycle (PM, perimenstrual; DF, dominant follicle developing; PO, periovulatory; CL, corpus luteum active; ND, no dominant structure apparent). # denotes trend differences ($P \leq 0.1$) between indicated groups; * denotes $P < 0.01$ between PM and DF. (**C**) Density of OSE cell Types, expressed as the number of cells per 250 μm of ovarian surface. * and ** denote $P < 0.05$ and $P < 0.01$, respectively, from Type 2. (**D**) Percentage of cells bearing an apical projection by type. ** denotes $P < 0.01$, compared with others. Error bars are the standard error of measurements from sampled FOV.

1.58 times higher than the percentage of positive cells farther from the dominant follicle. This was a statistical trend ($P = 0.07$) toward higher expression; however, this trend was not supported in all ovaries from this stage ($P = 0.43$).

Cadherin protein isoform expression during the primate menstrual cycle

The mean percentage of OSE cells on all ovaries that stained positive for E-, N-, P- and OB-cadherin were 48.7 ± 12.1, 3.3 ± 0.6, 53.1 ± 14.6 and 25.6 ± 10.3%, respectively. Each cadherin was detected in ovaries from all cycle stages, at variable levels. The source of this variability was not related to proximity to the dominant follicle or CL, or to morphological type of OSE. Furthermore, cadherin isoforms were not exclusive to regions of the ovarian surface, but commonly overlapped. E-cadherin decreased significantly ($P < 0.05$) from PM to DF (Fig. 4A), and other cadherins tended to decrease between PM and DF or PO (Fig. 4B–D). P-cadherin rose significantly ($P < 0.05$) from PO to CL (Fig. 4C). Representative staining is shown (right, each panel). As negative controls, tissue sections were exposed to secondary antibody alone, which did not show appreciable non-specific reactivity (Fig. 4C and D, lower right panels). When cadherin isoform expression data were normalized to values at menstruation (PM) and pooled for all cadherins, a significant ($P < 0.05$) decrease was seen between PM and both DF and PO stages; meanwhile a trend ($P = 0.07$) increase from PO to CL was observed (Fig. 4E).

Estrogen and progesterone receptors in the primate OSE

Nuclear receptors for E and P, ER-α and PR, were detected in the primate OSE, as was the cytoplasmic membrane-associated progesterone receptor PGRMC1 (Fig. 5A). ER-β was not detected (negative data not shown). Overall, ER-α, PR and PGRMC1 staining was detected in 22.0 ± 8.1, 56.9 ± 18.2 and 68.0 ± 5.8% of all OSE cells, respectively. The percentage of positive-staining cells did not correlate with proximity to the dominant follicle or CL, or to morphological type of OSE; however, ER-α-positive cells declined significantly

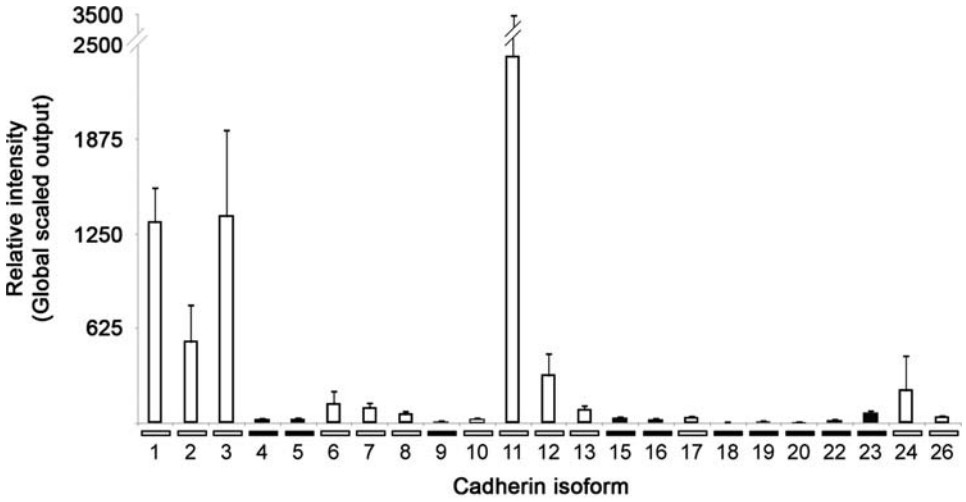

CDH	ProbeSet ID	ProbeSet Description
1	MmuSTS.3395.1.S1_at	gi:47776471
2	MmuSTS.1855.1.S1_at	gi:49533106
3	MmuSTS.3610.1.S1_at	gi:51853673
4	MmugDNA.14992.1.S1_at	gDNA.g4502724
5	MmuSTS.3396.1.S1_at	gi:47776472
6	MmugDNA.36879.1.S1_at	gDNA.Hs.32963.0.S1
7	MmuSTS.1856.1.S1_at	gi:49533107
8	MmuSTS.3613.1.S1_at	gi:51853674
9	MmuSTS.3398.1.S1_at	gi:47776474
10	MmuSTS.3381.1.S1_at	gi:47776467
11	MmuSTS.3607.1.S1_at	gi:51853672
12	MmuSTS.3382.1.S1_at	gi:47776468
13	MmuSTS.1984.1.S1_at	gi:47155546
15	MmugDNA.16368.1.S1_at	gDNA.g4826668
16	MmugDNA.6450.1.S1_at	gDNA.g4757955
17	MmuSTS.3383.1.S1_at	gi:47776469
18	MmuSTS.3394.1.S1_at	gi:47776470
19	MmuSTS.578.1.S1_at	gi:52626892
20	MmuSTS.579.1.S1_at	gi:52626893
22	MmugDNA.9740.1.S1_at	gDNA.Hs.264157.0.S1
23	MmugDNA.19234.1.S1_at	gDNA.Hs.244343.1.S1
24	MmugDNA.36559.1.S1_at	gDNA.Hs.155912.0.S1
26	MmuSTS.580.1.S1_at	gi:52626894

Figure 2 Transcriptional profile of mRNA levels for different cadherin isoforms in the primate OSE *in vivo*. Histogram shows the mean global-scaled, RMA-normalized fluorescent signal obtained from each chip ($n = 3$) hybridized with labeled OSE cDNA. Error bars are the standard error of measurements from RNA samples from three monkeys. Open bars indicate transcripts defined as 'present' while filled bars represent 'absent' transcripts. Table lists each Affymetrix probe set ID and description.

($P < 0.05$) between PO and CL stages (Fig. 5B), and the percentage of PR-positive cells showed a significant ($P < 0.05$) decline between PM and DF (Fig. 5C). The percentage of PGRMC1-positive cells did not change significantly during the menstrual cycle (Fig. 5D).

Proliferation in the primate OSE

Antibodies to detect proliferative potential or mitosis revealed only low levels of activity within the OSE (Fig. 6A–C). PCNA, pH3 and pRb staining was found in only 0.22 ± 0.11, 0.08 ± 0.14 and 0.02 ± 0.01% of OSE cells, respectively. No significant changes were observed in relation to the dominant follicle, CL or phase of the menstrual cycle (Fig. 6A–C). Evidence of proliferation could be detected in all morphological types of OSE cells, consistent with previous findings in which proliferation was induced by physical disruption of the OSE; in this prior study, markers of proliferation were detected at a frequency ~10-fold higher than seen here (Wright *et al.*, 2008). By way of comparison, the percentage of PCNA, pH3 and pRb-positive cells in preantral follicles was significantly ($P < 0.01$) higher than in the OSE. In many instances, several OSE cells in a single section were positive for these antigens. However, these cells were usually not clustered within 500 μm of each other.

Cell cycle arrest and apoptotic indicators in the primate OSE

p21, a mediator of cell cycle arrest, was detected in the OSE (Fig. 7A). Although no correlation was apparent in relation to the dominant follicle or CL, a significantly ($P < 0.05$) higher percentage of OSE-positive cells was seen during PM when compared with all other stages. Staining for the apoptotic mediator p53 was detected in the OSE, with a non-significant increase ($P = 0.08$) seen during DF versus other stages of the cycle; no significant changes were seen in relation to the dominant follicle or CL (Fig. 7B). The cleaved (active) form of caspase-3 mediates cell death, and was detected in the OSE (Fig. 7C). Cleaved caspase-3 may ($P = 0.07$) be higher during PM,

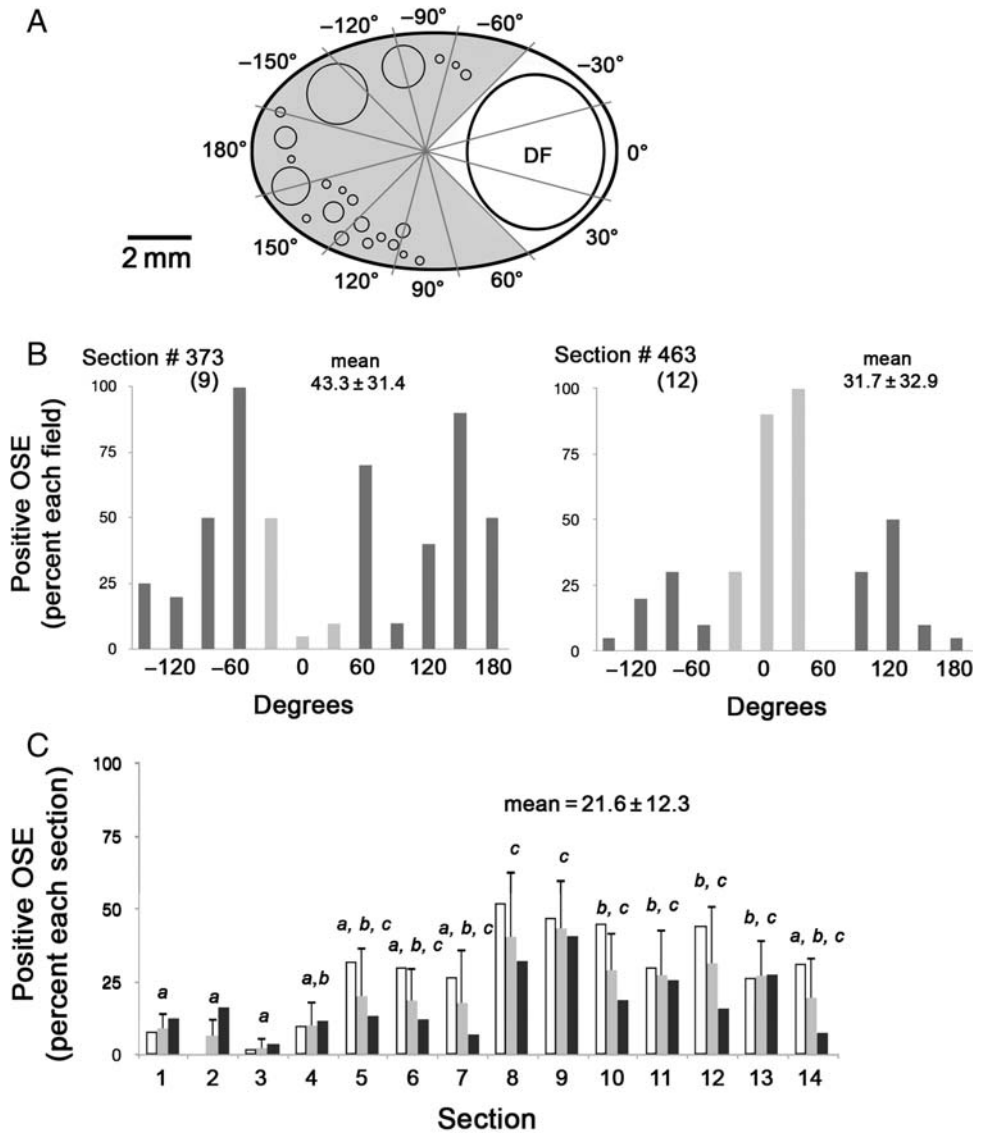

Figure 3 E-cadherin protein expression in the OSE of a single ovary at the DF stage. (**A**) Diagram showing a tissue section with a dominant follicle (DF), typically about 5 mm in diameter, and radial intervals around the section, approximating the FOV. Lighter intervals correspond to areas where the surface is defined as near the DF; darker intervals are considered to contain surface away from the DF. Unlabeled circles represent the pool of follicles in the ovarian cortex that will give rise to future ovulatory follicles. (**B**) Percentage of OSE cells expressing E-cadherin in each FOV in sections 373 and 463, numbered 9 and 12 in (**C**), below. These were selected from 14 sections spanning the entire ovary for illustrative purposes. Lighter bars are near the DF, darker bars are away from the DF. (C) Percentage of E-cadherin-positive cells in each of the 14 sections spanning the entire ovary. Values for each section are segregated on the basis of proximity to the DF: open bars are near the DF, black bars are distant to the DF; shaded bars are the average of all FOV in each section. Letters and error bars relate to the average values for each FOV. Different letters denote sections with significantly different levels ($P < 0.05$). Error bars are the standard error of measurements from FOV in each section.

relative to DF and PO (Fig. 7C). When PM and CL results were pooled and compared with DF and PO pooled data, cleaved caspase-3 was found in a significantly ($P < 0.05$) greater percentage of OSE cells during PM and CL stages, versus DF and PO stages. No significant association with proximity to the dominant follicle or CL was observed. The mean overall expression of p21, p53 and cleaved caspase-3 was 0.06 ± 0.07, 0.88 ± 1.1 and 0.08 ± 0.11% of all OSE cells, respectively. Each of these antigens was readily detected in luteal tissue, in significantly ($P < 0.01$) greater percentages of cells, compared with the OSE.

Mediators of DNA repair in the primate OSE

Immunostaining for FANCD2, a member of the Fanconi anemia and BRCA1/2 DNA repair families, and Ogg1, a mediator of DNA base repair, was detected in the primate OSE (Fig. 8). The general expression levels of FANCD2 and Ogg1 were 13.8 ± 3.9

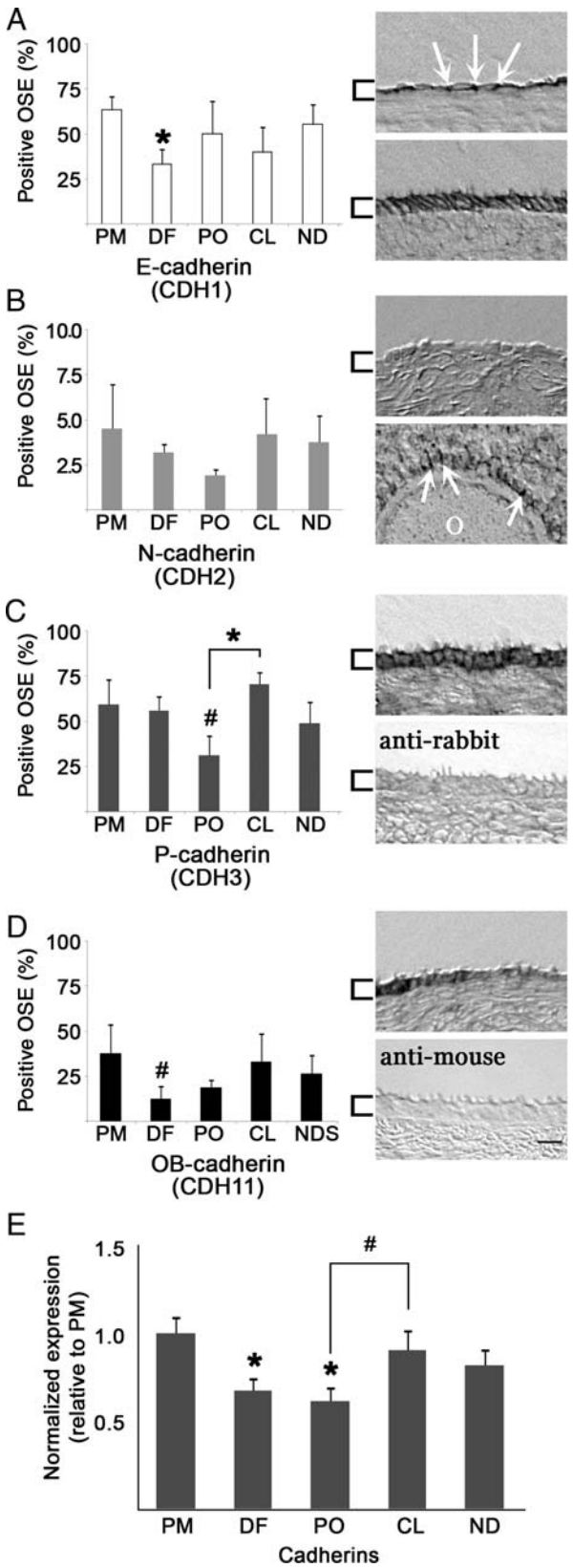

and 48.4 ± 3.3% of OSE cells, respectively. No significant changes were seen in relation to the dominant follicle or CL, or to morphological type of OSE. FANCD2 was seen in significantly ($P < 0.05$) more cells in DF than CL. These proteins were expressed at significantly ($P < 0.01$) lower levels in luteal tissue versus OSE.

The OSE at the follicle apex and after ovulation

A detailed visual inspection of PO ovaries was conducted to more stringently assess the OSE at the apex of the pre-ovulatory follicle (Fig. 9A), within 150 μm of the site of ovulation (Fig. 9B), and at the ovulatory stigma (Fig. 9C). Over the apex of the unruptured follicle, where the distance between the ovarian surface and follicle wall was only 60 μm, OSE cells of Type 2 morphology were most common. Type 1 cells were also detected, but not Type 3. Elevated levels of proliferation or cell death were not observed. After follicle rupture, the tunica albuginea between the OSE and luteinizing follicle wall decreased in thickness near the site of rupture, to <20 μm. Immediately at the rupture site, the tunic was displaced by debris, cells and fluid released from the follicle. Markers for the OSE were detected within 20 μm of the rupture site. H&E staining of putative OSE cells within this region showed some amount of disorder, manifesting as gaps between surface cells and a rounded morphology. OSE cells beyond this narrow range (>20 μm) showed no comparable alterations. The presence of a small number of OSE–marker-expressing cells atop the ovulatory stigma provided evidence that OSE cells may be displaced by ovulation; however, the fate of these cells could not be definitively established: due to the high level of expression of markers for proliferation, cell cycle arrest and death within the luteinizing tissue, detection of these markers at the stigma surface could not be assigned with confidence to displaced OSE cells.

Figure 4 Cadherin isoform expression in the OSE during the menstrual cycle. Histograms (**A**–**D**, left panels; **E**) show mean expression levels in the OSE during each defined stage. Data are mean ± standard error for $n \geq 3$ sections per ovary. Images (right panels) show labeling for each isoform antibody, or negative control, as indicated. Arrows highlight regions of cell–cell contact; brackets highlight the OSE; scale bar = 10 μm. (**A**) E-cadherin: upper panel presents Type 1 cells, lower panel shows Type 3 cells. (**B**) N-cadherin: upper panel shows OSE, lower panel demonstrates expression in granulosa cells surrounding the oocyte (O) of a pre-antral follicle. (C) P-cadherin: upper panel shows OSE cells; lower panel represents a negative control: tissue labeled only with secondary anti-rabbit antibody. (D) OB-cadherin: upper panel shows OSE; lower panel shows tissue labeled only with secondary anti-mouse antibody. (**E**) Pooled expression of all cadherins, normalized to PM stage values. * denotes $P < 0.05$ relative to PM expression, or as indicated; # denotes trending differences ($P \leq 0.1$) relative to PM, or as indicated.

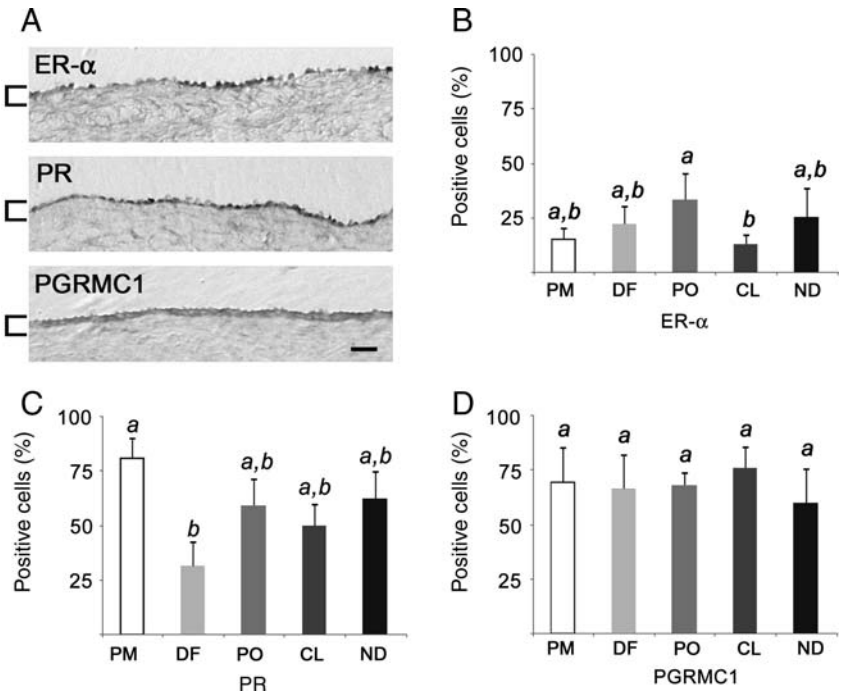

Figure 5 ER-α, PR and PGRMC1 expression in the primate OSE. (**A**) Antibody staining for each receptor. Brackets highlight the OSE; scale bar = 15 μm. (**B**–**D**) Percentage of positive cells for each receptor at each stage. Different letters denote significantly different levels ($P < 0.05$). Error bars are the standard error of mean values from sections ($n \geq 3$) from each ovary ($n \geq 3$) at each stage.

Discussion

The primate OSE displays cycle-independent and cycle-dependent properties that distinguish it from other ovarian cell types and suggest diverse influences from the menstrual cycle; however, proximity to the dominant follicle selected to ovulate or the CL did not clearly affect the OSE. Cycle-independent properties of the OSE include low basal rates of proliferation, with no evidence of fixed loci or beds of OSE progenitor (stem) cells, and a higher percentage of cells expressing DNA repair proteins, relative to granulosa and luteal cells. It is possible that the ovary suppresses basal proliferation (PCNA, pH3 and pRb), or at least the expression of markers of proliferation, within the OSE and induces higher levels of DNA repair potential (FANCD2 and Ogg1). Alternatively, these may be ovary-independent properties of the OSE that minimize proliferation of cells that are routinely damaged. Future studies to manipulate the OSE and its local ovarian environment *in vivo* may more effectively evaluate these possibilities. Notably, luteal cells die as the CL functionally and structurally regresses, typically within days, and it could be argued that they express less DNA repair potential based on the absence of a need for survival; likewise, a survey of antral follicles (≥0.2 mm in diameter) revealed FANCD2 or Ogg1 in generally fewer than 5% of granulosa or thecal cells (data not shown), and some antral follicles survive for weeks.

Cycle-dependent changes seen in the OSE were generally modest, but significant: (i) the distribution of morphological types shifted between PM and DF stages, with a gain of Type 2 and possible loss of Type 3 cells; (ii) the percentage of cadherin-expressing cells was generally lower during DF and PO than in CL and PM stages; (iii) the frequency of ER-α-positive cells declined between PO and CL, coinciding with a transition between an estrogen- versus progesterone-dominated milieu; (iv) PR expression declined significantly after PM; (v) p21, a mediator of cell cycle arrest, was significantly higher during PM than all other stages of the cycle; (vi) cleaved caspase-3, an effector of cell death, was significantly higher during PO and CL, and; (viii) FANCD2 was highest during DF and lowest during CL. These findings suggest the ovary influences OSE adhesion, steroid responsiveness, cell cycle, death and DNA damage repair during the menstrual cycle, albeit to a limited extent and not uniformly throughout the OSE.

A deeper level of analysis is warranted in future studies. While we were able to demonstrate that, for example, cadherin isoform expression did not clearly determine morphological type or proliferative activity, and that morphological type did not define which cells expressed markers of proliferation, other correlations could not be confidently investigated, given the sample size of the current study, and the low frequencies of some of the antigens detected here. In order to unravel mechanisms controlling the OSE during the natural cycle, it will be important to identify *in vivo* functional interactions between the pathways represented by proteins studied here, as well as other molecules, such as matrix remodeling enzymes, mediators of inflammation and growth factor receptors.

Investigating the OSE overlying the emerging pre-ovulatory follicle and surrounding the site of ovulation reinforced the conclusion that the primate OSE is generally stable, possibly resistant to ovulation-associated DNA damage, and less influenced by proximity

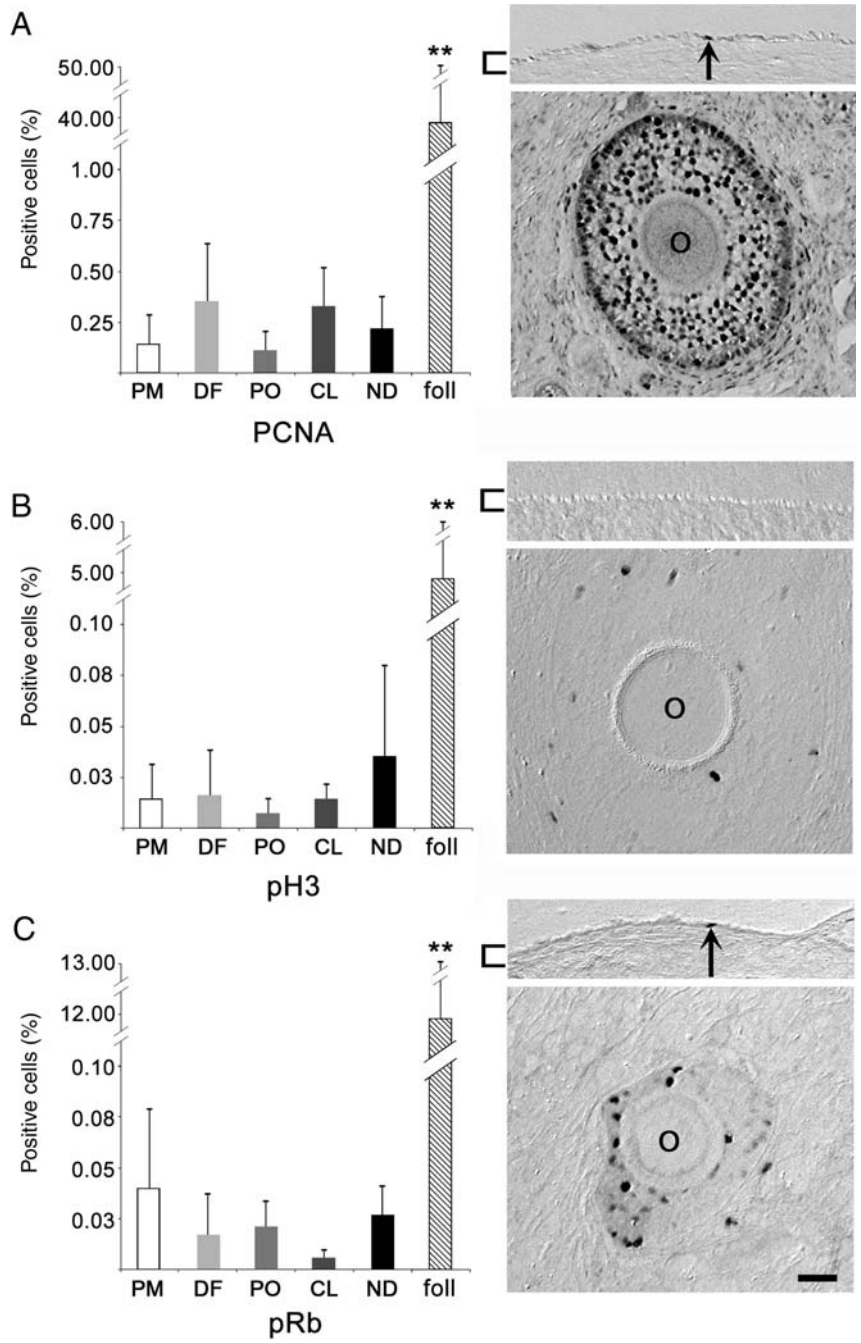

Figure 6 Antibody labeling to detect proliferative activity in the primate OSE during the menstrual cycle. Percentage of positive OSE cells (left panels) labeled for (**A**) PCNA, (**B**) pH3 and (**C**) pRb. Expression in pre-antral follicles (foll; $n = 3$) is shown for comparison. ** denotes $P < 0.01$. Images (right panels) show the OSE (upper) or a pre-antral follicle (lower). O = oocyte; brackets highlight the OSE; arrows indicate positive OSE cells; scale bar = 15 μm.

to the dominant structures than was expected. At the pre-ovulatory stage, the follicle apex displayed OSE that was statistically indistinguishable from OSE distant from the apex. However, after follicle rupture, the OSE within 20 μm of the ovulatory site showed signs of disorder, but not apoptosis or proliferation. This study may not have the temporal resolution necessary to detect brief, narrowly localized changes in the OSE. Cellular events prior to follicle rupture may occur within a span of hours—perhaps <1% of the entire cycle (Colgin and Murdoch, 1997). Staging ovaries precisely in the PO interval is difficult within the natural cycle, but is possible using a controlled ovulation protocol that permits tissue collection at precise time increments after administering an ovulatory bolus of hCG (Young *et al.*, 2003). It will be important to conduct precisely timed studies to resolve the fate of the primate OSE at ovulation: dissolution of the tunica

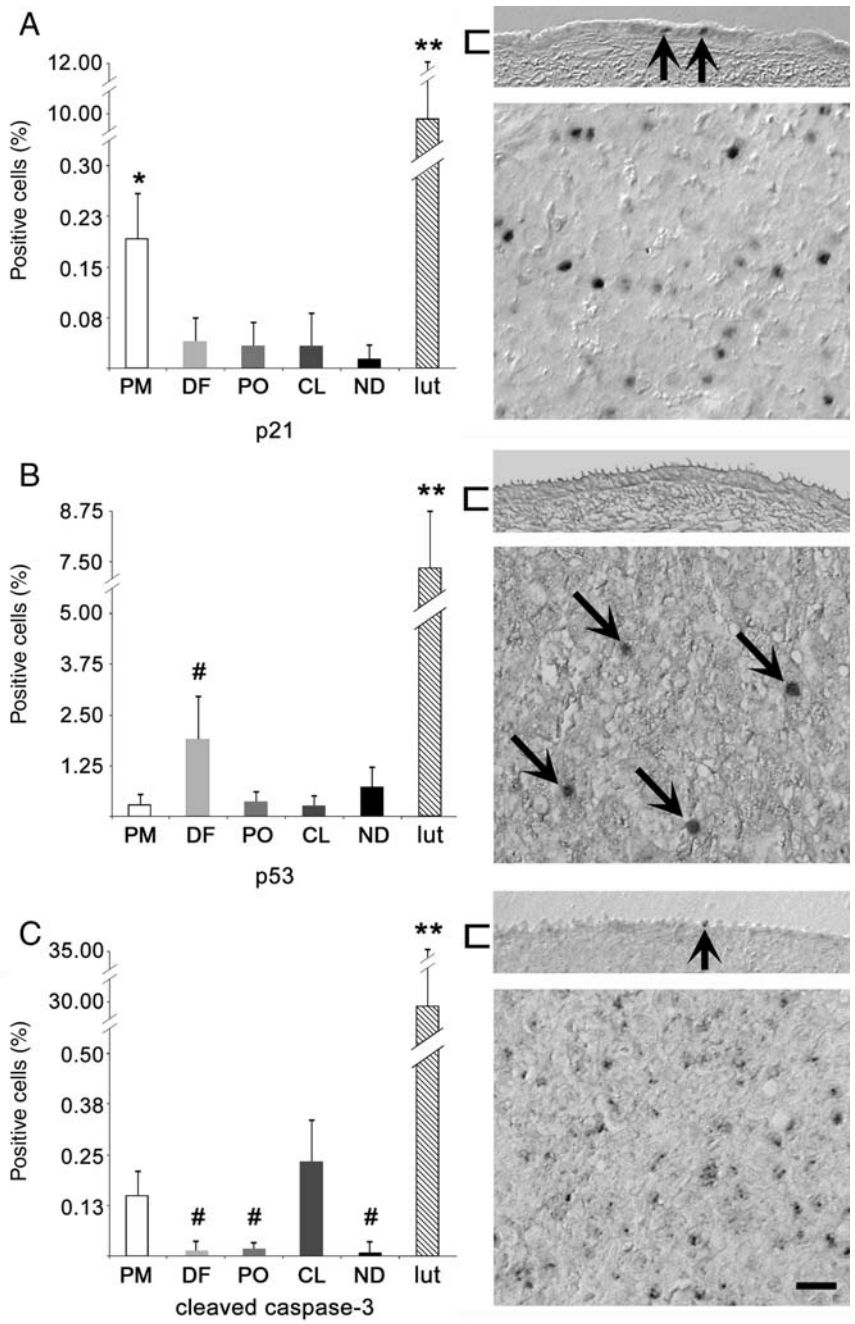

Figure 7 Antibody labeling to detect cell cycle arrest and apoptotic potential. Percentage of positive OSE cells (left panels) labeled for (**A**) p21, (**B**) p53 and (**C**) cleaved caspase-3. Expression in Day 21 luteal tissue (lut; $n = 3$) is shown for comparison. * and ** denote $P < 0.05$ between OSE of other stages and $P < 0.01$ from OSE of all stages; # denotes trending differences ($P \leq 0.1$) relative to PM (B) or PM and CL (C). Images (right panels) show the OSE (upper) or luteal tissue (lower). Brackets highlight the OSE; arrows indicate positive OSE or luteal cells; scale bar = 15 μm.

albuginea underlying the OSE at the rupture site, and/or subsequent exposure to follicle contents could trigger OSE death, while leaving OSE attached to the tunic intact; alternatively, OSE cells separated from the tunic could escape death and be transported away from the ovary, along with follicular contents, and be deposited within the reproductive tract or peritoneal cavity. The diameter of the stigma in rhesus macaques can span several millimeters (Wright *et al.*, 2010), so the potential exists for a large number of cells to be shed from the ovary during each ovulation. Those surviving deposition could face an environment that fails to suppress proliferation and promote DNA repair, thus increasing malignant potential. Future studies detailing follicle rupture may reveal rapid loss of OSE where

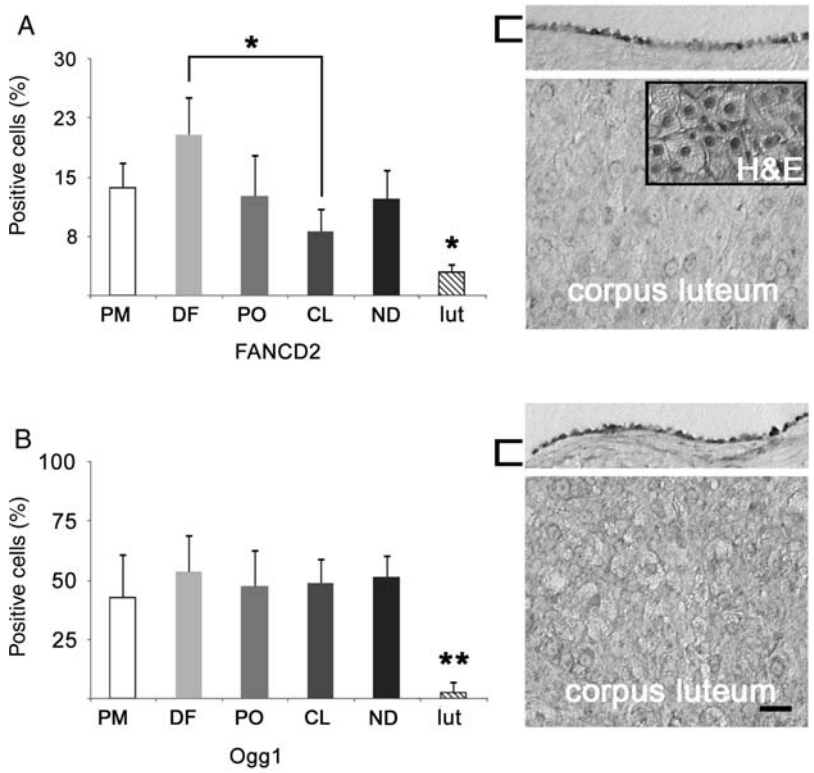

Figure 8 IHC detection of DNA repair proteins in the primate OSE during the menstrual cycle. Evaluation of (**A**) FANCD2 and (**B**) Ogg1. Expression in Day 21 luteal tissue (lut; $n = 3$) is shown for comparison. Histograms (left) show the percentage of positive cells $\pm$ the standard error. * and ** denote $P < 0.05$ and $P < 0.01$, respectively, between luteal tissue and OSE, or between stages, as indicated. For images (right), the upper panels represent the OSE and the lower show luteal tissue. Inset is H&E staining of an adjacent section. Brackets highlight the OSE; scale bar = 15 μm.

the ovarian tunic is obliterated during ovulation. This would indicate greater agreement with findings from other model systems, especially the well-studied ovine model (Murdoch and McDonnel, 2002), than reported here.

The presence of FANCD2 at higher levels in the OSE than in other ovarian cell types supports the concept of a pathway to transformation beginning with defective DNA repair. The Fanconi anemia/BRCA pathway is strongly associated with familial breast and ovarian cancer due to mutations in BRCA1 or 2 (Lynch *et al.*, 2009), but loss of FANCD2 could also disrupt this pathway and result in EOC. Interestingly, FANCD2 expression is decreased in OSE, but not other cell types, from many women with a family history of the disease (Pejovic *et al.*, 2006). Novel strategies for early detection or prevention of EOC may include screening for epigenetic defects in this pathway or developing methods to preserve DNA repair mechanisms in the OSE. Other DNA repair mechanisms appear to act on the ovine OSE at the site of ovulation, including polymerase-beta and poly(ADP-ribose) polymerase (Murdoch, 2005), and this encourages a more extensive study of additional repair mechanisms in the primate OSE.

The current findings are consistent with prevailing perspectives on EOC etiology to greater or lesser degrees. The underlying basis for the 'Incessant Ovulation' hypothesis (Fathalla, 1971) is not well supported here, owing to the lack of proliferation at the site of ovulation. It has yet to be determined whether the diameter of the ovulatory site correlates to the amount of tunica albuginea (and OSE) that must be replaced. The damage to the tunic may hypothetically be repaired in large part by contraction of the ovarian surface as the CL regresses; if so, the need for proliferative repair of the OSE may be minimal. Other aspects of ovulation may contribute to cancer risk, including the displacement of OSE cells. The role of sex steroids is supported by the expression of ER-α, PR and PGRMC1 and OSE death rates that rise, modestly but significantly, during periods of P production. The importance of inflammation is also supported, by the expression of glucocorticoid receptors and metabolic enzymes, not reported here, that may mediate proliferation, attenuate local inflammatory damage and protect the genome [e.g. 11bHSD1 and 2, and IL-1R; (Syed *et al.*, 2001; Gubbay *et al.*, 2004; Rae *et al.*, 2004; Fegan *et al.*, 2008) and unpublished microarray and IHC observations].

The primate OSE appears to differ from that of non-primates including mouse, rat, guinea pig, sheep and hen, particularly in terms of proliferation and cell death, steroid receptor expression patterns and the lack of roles in ovulation or preventing adhesions (Osterholzer *et al.*, 1985; Isola *et al.*, 1987; Gillett *et al.*, 1994; Colgin and Murdoch, 1997; Murdoch *et al.*, 2001; Murdoch and McDonnel, 2002; Symonds *et al.*, 2003; Murdoch and Martinchick, 2004; Tan and Fleming, 2004; Gaytan *et al.*, 2005). Many of these differences may be only a matter of degree, and factors that predispose the primate OSE to malignant

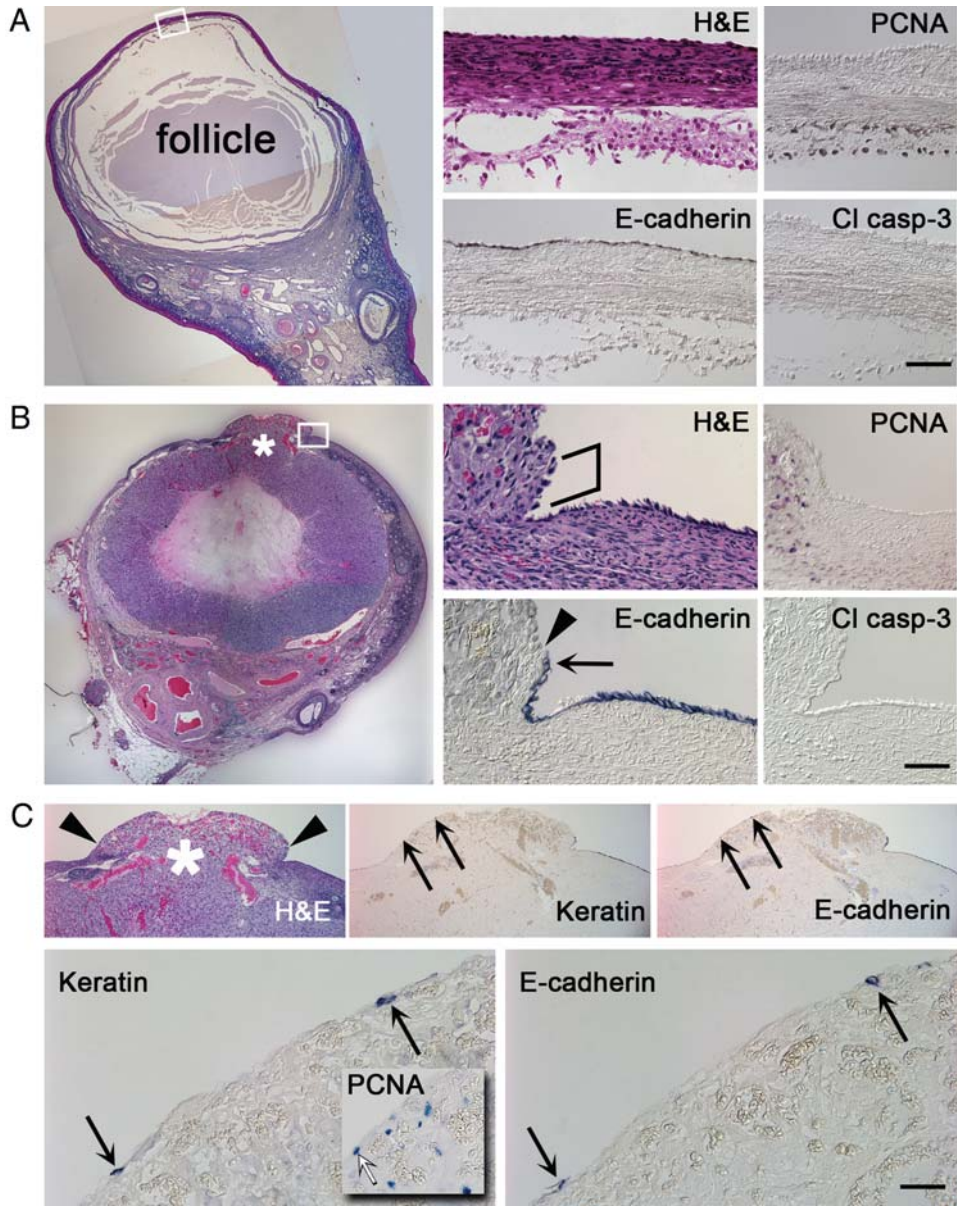

Figure 9 Evaluation of the primate OSE in relation to the dominant follicle selected to ovulate and to the developing CL. (**A**) A DF stage ovary labeled with H&E (left) shows the unruptured pre-ovulatory follicle. Higher magnification images corresponding to the boxed region are included (middle and right). The top portion of each panel depicts the ovarian surface, while the bottom portion shows follicular cells and antrum. Scale bar = 1.0 mm and 25 μm for the lower and higher magnification panels, respectively. (**B**) A CL stage ovary labeled with H&E (left) shows a ruptured, luteinizing follicle. Higher magnification images corresponding to the boxed region are shown (middle and right). An asterisk (*) marks the site of ovulation. Irregular bracket highlights a span of widely spaced putative OSE cells adjacent to luteal tissue. Arrowhead indicates the approximate demarkation between the tunica albuginea and ruptured luteinizing follicle. Arrow indicates E-cadherin label closest to the rupture site. Scale bar = 1.0 mm and 25 μm for the lower and higher magnification panels, respectively. (**C**) The ovulatory stigma shown in (B). Arrowheads indicate the approximate demarkation between luteal tissue and ovarian surface. * denotes the rupture site. Keratin- and E-cadherin-labeled sections are shown, with higher magnification included (bottom panels). Arrows indicate possible OSE cells, pointing to the same locations in lower versus higher magnification panels; inset shows PCNA labeling; white arrow indicates a PCNA-positive cell at the stigma surface. Scale bar = 0.5 mm and 10 μm in top and bottom panels, respectively.

transformation may not be inherent to the OSE, but to its broader biological context. It is unknown whether a comprehensive study of ovaries from healthy, cycling women would reveal an OSE more similar to rhesus macaque OSE than to non-primate OSE. Such a study has ethical and practical limitations, but would help to establish the relative value of future non-human primate studies. While chemically and genetically engineered rodent models of EOC [reviewed in (Garson *et al.*, 2005; Fong and Kakar, 2009)] and spontaneously

occurring cancer in the hen (Fredrickson, 1987; Johnson, 2009) are powerful and valuable resources, the results of this study suggest a non-human primate model may be uniquely suited for representing the normal OSE of women and investigating the preceding and early stages of EOC. Likewise, due to the likelihood that a significant number of pelvic tumors diagnosed as EOC may originate within the fallopian tube or fimbria, primarily in BRCA1 mutation carriers, but also in the general population (Medeiros *et al*., 2006; Folkins *et al*., 2009; Shaw *et al*., 2009), a model to investigate the FE during the menstrual cycle, and in relation to age, could help resolve the origins of EOC. The rhesus macaque is similarly well-suited to investigate the normal fallopian tube and fimbria as it is to study the normal OSE. Thus, the non-human primate may allow more effective development of strategies to improve EOC outcomes prior to disease onset or during early stages of progression.

Authors' roles

J.W.W.: contributed to study conception and design, execution and analysis, manuscript preparation and critical review and final manuscript approval. L.J.: contributed to data collection and interpretation, protocol design, critical manuscript review and final manuscript approval. R.L.S. contributed to study conception and design, data interpretation and analytic approach, critical manuscript revision and discussion and final manuscript approval.

Funding

This work was supported by NIH HD050356 (J.W.W.), NIH/NCRR RR000163 and NIH HD18185 (R.L.S.)

References

Auersperg N, Woo MM, Gilks CB. The origin of ovarian carcinomas: a developmental view. *Gynecol Oncol* 2008;**110**:452–454.

Bai W, Oliveros-Saunders B, Wang Q, Acevedo-Duncan ME, Nicosia SV. Estrogen stimulation of ovarian surface epithelial cell proliferation. *In Vitro Cell Dev Biol Anim* 2000;**36**:657–666.

Bellino FL, Wise PM. Nonhuman primate models of menopause workshop. *Biol Reprod* 2003;**68**:10–18.

Bogan RL, Murphy MJ, Stouffer RL, Hennebold JD. Systematic determination of differential gene expression in the primate corpus luteum during the luteal phase of the menstrual cycle. *Mol Endocrinol* 2008;**22**:1260–1273.

Bowen NJ, Walker LD, Matyunina LV, Logani S, Totten KA, Benigno BB, McDonald JF. Gene expression profiling supports the hypothesis that human ovarian surface epithelia are multipotent and capable of serving as ovarian cancer initiating cells. *BMC Med Genomics* 2009;**2**:71.

Burdette JE, Kurley SJ, Kilen SM, Mayo KE, Woodruff TK. Gonadotropin-induced superovulation drives ovarian surface epithelia proliferation in CD1 mice. *Endocrinology* 2006;**147**:2338–2345.

Burdette JE, Oliver RM, Ulyanov V, Kilen SM, Mayo KE, Woodruff TK. Ovarian epithelial inclusion cysts in chronically superovulated CD1 and Smad2 dominant-negative mice. *Endocrinology* 2007;**148**:3595–3604.

Chaffin CL, Stouffer RL, Duffy DM. Gonadotropin and steroid regulation of steroid receptor and aryl hydrocarbon receptor messenger ribonucleic acid in macaque granulosa cells during the periovulatory interval. *Endocrinology* 1999;**140**:4753–4760.

Colgin DC, Murdoch WJ. Evidence for a role of the ovarian surface epithelium in the ovulatory mechanism of the sheep: secretion of urokinase-type plasminogen activator. *Anim Reprod Sci* 1997;**47**:197–204.

Davies BR, Finnigan DS, Smith SK, Ponder BA. Administration of gonadotropins stimulates proliferation of normal mouse ovarian surface epithelium. *Gynecol Endocrinol* 1999;**13**:75–81.

Doyle LK, Donadeu FX. Regulation of the proliferative activity of ovarian surface epithelial cells by follicular fluid. *Anim Reprod Sci* 2009;**114**:443–448.

Fathalla MF. Incessant ovulation—a factor in ovarian neoplasia?. *Lancet* 1971;**2**:163.

Fegan KS, Rae MT, Critchley HO, Hillier SG. Anti-inflammatory steroid signalling in the human peritoneum. *J Endocrinol* 2008;**196**:369–376.

Folkins AK, Saleemuddin A, Garrett LA, Garber JE, Muto MG, Tworoger SS, Crum CP. Epidemiologic correlates of ovarian cortical inclusion cysts (CICs) support a dual precursor pathway to pelvic epithelial cancer. *Gynecol Oncol* 2009;**115**:108–111.

Fong MY, Kakar SS. Ovarian cancer mouse models: a summary of current models and their limitations. *J Ovarian Res* 2009;**2**:12.

Fredrickson TN. Ovarian tumors of the hen. *Environ Health Perspect* 1987;**73**:35–51.

Garson K, Shaw TJ, Clark KV, Yao DS, Vanderhyden BC. Models of ovarian cancer—are we there yet?. *Mol Cell Endocrinol* 2005;**239**:15–26.

Gaytan M, Sanchez MA, Morales C, Bellido C, Millan Y, Martin de Las Mulas J, Sanchez-Criado JE, Gaytan F. Cyclic changes of the ovarian surface epithelium in the rat. *Reproduction* 2005;**129**:311–321.

Giles JR, Olson LM, Johnson PA. Characterization of ovarian surface epithelial cells from the hen: a unique model for ovarian cancer. *Exp Biol Med (Maywood)* 2006;**231**:1718–1725.

Gillett WR, James C, Jetha N, McComb PF. Removal of the ovarian surface epithelium from the rabbit ovary—a cause of adhesions following a standard injury. *Hum Reprod* 1994;**9**:497–500.

Gubbay O, Guo W, Rae MT, Niven D, Howie AF, McNeilly AS, Xu L, Hillier SG. Anti-inflammatory and proliferative responses in human and ovine ovarian surface epithelial cells. *Reproduction* 2004;**128**:607–614.

Gubbay O, Guo W, Rae MT, Niven D, Langdon SP, Hillier SG. Inflammation-associated gene expression is altered between normal human ovarian surface epithelial cells and cell lines derived from ovarian adenocarcinomas. *Br J Cancer* 2005;**92**:1927–1933.

Heller DS, Hameed M, Baergen R. Lack of proliferative activity of surface epithelial inclusion cysts of the ovary. *Int J Gynecol Cancer* 2003;**13**:303–307.

Heller DS, Murphy P, Westhoff C. Are germinal inclusion cysts markers of ovulation? *Gynecol Oncol* 2005;**96**:496–499.

Isola J, Korte JM, Tuohimaa P. Immunocytochemical localization of progesterone receptor in the chick ovary. *Endocrinology* 1987;**121**:1034–1040.

Ivarsson K, Sundfeldt K, Brannstrom M, Hellberg P, Janson PO. Diverse effects of FSH and LH on proliferation of human ovarian surface epithelial cells. *Hum Reprod* 2001;**16**:18–23.

Johnson KA. The standard of perfection: thoughts about the laying hen model of ovarian cancer. *Cancer Prev Res (Phila)* 2009;**2**:97–99.

Keith Bechtel M, Bonavida B. Inhibitory effects of 17beta-estradiol and progesterone on ovarian carcinoma cell proliferation: a potential role for inducible nitric oxide synthase. *Gynecol Oncol* 2001;**82**:127–138.

Lane MA, Black A, Handy AM, Shapses SA, Tilmont EM, Kiefer TL, Ingram DK, Roth GS. Energy restriction does not alter bone mineral metabolism or reproductive cycling and hormones in female rhesus monkeys. *J Nutr* 2001;**131**:820–827.

Lynch HT, Casey MJ, Snyder CL, Bewtra C, Lynch JF, Butts M, Godwin AK. Hereditary ovarian carcinoma: heterogeneity, molecular genetics, pathology, and management. *Mol Oncol* 2009;**3**:97–137.

Marquez RT, Baggerly KA, Patterson AP, Liu J, Broaddus R, Frumovitz M, Atkinson EN, Smith DI, Hartmann L, Fishman D *et al.* Patterns of gene expression in different histotypes of epithelial ovarian cancer correlate with those in normal fallopian tube, endometrium, and colon. *Clin Cancer Res* 2005;**11**:6116–6126.

Medeiros F, Muto MG, Lee Y, Elvin JA, Callahan MJ, Feltmate C, Garber JE, Cramer DW, Crum CP. The tubal fimbria is a preferred site for early adenocarcinoma in women with familial ovarian cancer syndrome. *Am J Surg Pathol* 2006;**30**:230–236.

Moore CM, Hubbard GB, Leland MM, Dunn BG, Best RG. Spontaneous ovarian tumors in twelve baboons: a review of ovarian neoplasms in non-human primates. *J Med Primatol* 2003;**32**:48–56.

Mukherjee K, Syed V, Ho SM. Estrogen-induced loss of progesterone receptor expression in normal and malignant ovarian surface epithelial cells. *Oncogene* 2005;**24**:4388–4400.

Murdoch WJ. Carcinogenic potential of ovulatory genotoxicity. *Biol Reprod* 2005;**73**:586–590.

Murdoch WJ, Martinchick JF. Oxidative damage to DNA of ovarian surface epithelial cells affected by ovulation: carcinogenic implication and chemoprevention. *Exp Biol Med (Maywood)* 2004;**229**:546–552.

Murdoch WJ, McDonnel AC. Roles of the ovarian surface epithelium in ovulation and carcinogenesis. *Reproduction* 2002;**123**:743–750.

Murdoch WJ, Townsend RS, McDonnel AC. Ovulation-induced DNA damage in ovarian surface epithelial cells of ewes: prospective regulatory mechanisms of repair/survival and apoptosis. *Biol Reprod* 2001;**65**:1417–1424.

NRC. *Guide for the Care and Use of Laboratory Animals*. Washington DC, USA, 1996.

Nichols SM, Bavister BD, Brenner CA, Didier PJ, Harrison RM, Kubisch HM. Ovarian senescence in the rhesus monkey (Macaca mulatta). *Hum Reprod* 2005;**20**:79–83.

Osterholzer HO, Johnson JH, Nicosia SV. An autoradiographic study of rabbit ovarian surface epithelium before and after ovulation. *Biol Reprod* 1985;**33**:729–738.

Parrott JA, Doraiswamy V, Kim G, Mosher R, Skinner MK. Expression and actions of both the follicle stimulating hormone receptor and the luteinizing hormone receptor in normal ovarian surface epithelium and ovarian cancer. *Mol Cell Endocrinol* 2001;**172**:213–222.

Pejovic T, Yates JE, Liu HY, Hays LE, Akkari Y, Torimaru Y, Keeble W, Rathbun RK, Rodgers WH, Bale AE *et al.* Cytogenetic instability in ovarian epithelial cells from women at risk of ovarian cancer. *Cancer Res* 2006;**66**:9017–9025.

Piek JM, Verheijen RH, Menko FH, Jongsma AP, Weegenaar J, Gille JJ, Pals G, Kenemans P, van Diest PJ. Expression of differentiation and proliferation related proteins in epithelium of prophylactically removed ovaries from women with a hereditary female adnexal cancer predisposition. *Histopathology* 2003;**43**:26–32.

Pothuri B, Leitao MM, Levine DA, Viale A, Olshen AB, Arroyo C, Bogomolniy F, Olvera N, Lin O, Soslow RA *et al.* Genetic analysis of the early natural history of epithelial ovarian carcinoma. *PLoS ONE* 2010;**5**:e10358.

Rae MT, Hillier SG. Steroid signalling in the ovarian surface epithelium. *Trends Endocrinol Metab* 2005;**16**:327–333.

Rae MT, Niven D, Critchley HO, Harlow CR, Hillier SG. Antiinflammatory steroid action in human ovarian surface epithelial cells. *J Clin Endocrinol Metab* 2004;**89**:4538–4544.

Resko JA, Goy RW, Robinson JA, Norman RL. The pubescent rhesus monkey: some characteristics of the menstrual cycle. *Biol Reprod* 1982;**27**:354–361.

Rodriguez GC, Nagarsheth NP, Lee KL, Bentley RC, Walmer DK, Cline M, Whitaker RS, Isner P, Berchuck A, Dodge RK *et al.* Progestin-induced apoptosis in the Macaque ovarian epithelium: differential regulation of transforming growth factor-beta. *J Natl Cancer Inst* 2002;**94**:50–60.

Shaw PA, Rouzbahman M, Pizer ES, Pintilie M, Begley H. Candidate serous cancer precursors in fallopian tube epithelium of BRCA1/2 mutation carriers. *Mod Pathol* 2009;**22**:1133–1138.

Slot KA, de Boer-Brouwer M, Voorendt M, Sie-Go DM, Ghahremani M, Dorrington JH, Teerds KJ. Irregularly shaped inclusion cysts display increased expression of Ki67, Fas, Fas ligand, and procaspase-3 but relatively little active caspase-3. *Int J Gynecol Cancer* 2006; **16**:231–239.

Sueblinvong T, Carney ME. Current understanding of risk factors for ovarian cancer. *Curr Treat Options Oncol* 2009;**10**:67–81.

Syed V, Ulinski G, Mok SC, Yiu GK, Ho SM. Expression of gonadotropin receptor and growth responses to key reproductive hormones in normal and malignant human ovarian surface epithelial cells. *Cancer Res* 2001;**61**:6768–6776.

Symonds D, Tomic D, Borgeest C, McGee E, Flaws JA. Smad 3 regulates proliferation of the mouse ovarian surface epithelium. *Anat Rec A Discov Mol Cell Evol Biol* 2003;**273**:681–686.

Tan OL, Fleming JS. Proliferating cell nuclear antigen immunoreactivity in the ovarian surface epithelium of mice of varying ages and total lifetime ovulation number following ovulation. *Biol Reprod* 2004; **71**:1501–1507.

Tan OL, Hurst PR, Fleming JS. Location of inclusion cysts in mouse ovaries in relation to age, pregnancy, and total ovulation number: implications for ovarian cancer? *J Pathol* 2005;**205**:483–490.

Walker ML, Herndon JG. Menopause in nonhuman primates? *Biol Reprod* 2008;**79**:398–406.

Werness BA, Afify AM, Eltabbakh GH, Huelsman K, Piver MS, Paterson JM. p53, c-erbB, and Ki-67 expression in ovaries removed prophylactically from women with a family history of ovarian cancer. *Int J Gynecol Pathol* 1999;**18**:338–343.

Westhoff C, Murphy P, Heller D, Halim A. Is ovarian cancer associated with an increased frequency of germinal inclusion cysts? *Am J Epidemiol* 1993;**138**:90–93.

Wolf DP, Thomson JA, Zelinski-Wooten MB, Stouffer RL. In vitro fertilization-embryo transfer in nonhuman primates: the technique and its applications. *Mol Reprod Dev* 1990;**27**:261–280.

Wong AS, Auersperg N. Ovarian surface epithelium: family history and early events in ovarian cancer. *Reprod Biol Endocrinol* 2003; **1**:70.

Wright JW, Stouffer RL, Rodland KD. High-dose estrogen and clinical selective estrogen receptor modulators induce growth arrest, p21, and p53 in primate ovarian surface epithelial cells. *J Clin Endocrinol Metab* 2005;**90**:3688–3695.

Wright JW, Pejovic T, Fanton J, Stouffer RL. Induction of proliferation in the primate ovarian surface epithelium in vivo. *Hum Reprod* 2008; **23**:129–138.

Wright JW, Pejovic T, Lawson M, Jurevic L, Hobbs T, Stouffer RL. Ovulation in the absence of the ovarian surface epithelium in the primate. *Biol Reprod* 2010;**82**:599–605.

Young KA, Hennebold JD, Stouffer RL. Dynamic expression of mRNAs and proteins for matrix metalloproteinases and their tissue inhibitors in the primate corpus luteum during the menstrual cycle. *Mol Hum Reprod* 2002;**8**:833–840.

Young KA, Chaffin CL, Molskness TA, Stouffer RL. Controlled ovulation of the dominant follicle: a critical role for LH in the late follicular phase of the menstrual cycle. *Hum Reprod* 2003; **18**:2257–2263.